Article published online: 2020-10-28

Liquid Crystalline Benzoic Acid Ester MIDA Boronates: Synthesis and Mesomorphic Properties

Christopher Schilling[a]
Finn Schulz[a]
Andreas Köhn[b]
Sabine Laschat*[a]

[a] Institut für Organische Chemie, Universität Stuttgart, Pfaffenwaldring 55, 70569 Stuttgart, Germany
[b] Institut für Theoretische Chemie, Universität Stuttgart, Pfaffenwaldring 55, 70569 Stuttgart, Germany
sabine.laschat@oc.uni-stuttgart.de

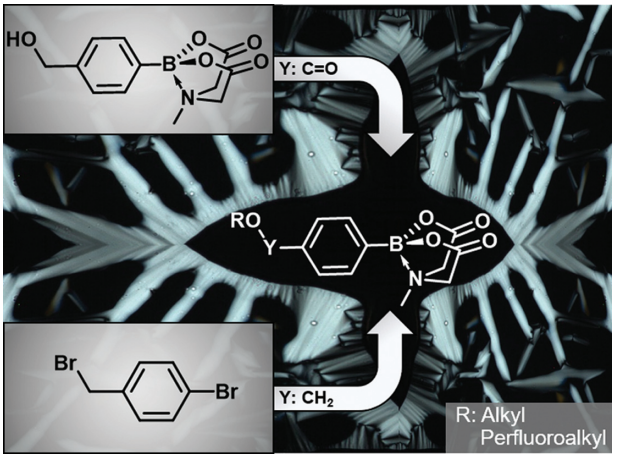

Received: 3.06.2020
Accepted after revision: 9.07.2020
DOI: 10.1055/s-0040-1715900; Art ID: om-20-0021oa

License terms:

© 2020. The Author(s). This is an open access article published by Thieme under the terms of the Creative Commons Attribution License, permitting unrestricted use, distribution, and reproduction so long as the original work is properly cited. (https://creativecommons.org/licenses/by/4.0/)

Abstract Two series of *N*-methyliminodiacetic acid (MIDA) boronates were prepared and their mesomorphic properties were investigated. MIDA-substituted benzoic acid esters were synthesized via the Mitsunobu reaction. The second series of MIDA benzyl ether derivatives was prepared via Williamson etherification and subsequent borylation. Both series exhibit smectic A (SmA) phases. In the case of MIDA boronate esters, a substitution with perfluorinated side chains led to increased transition temperatures and broadening of the SmA phases. The phase geometries of the mesophases were determined by X-ray diffraction. Quantum-chemical calculations provided further insight into the packing model.

Key words boronate, MIDA, liquid crystals, mesophases, Mitsunobu reaction

Introduction

Boron-containing liquid crystals are an emerging class of soft matter materials. Particular emphasis has been put on borondipyrromethane (BODIPY) derivatives,[1–12] borondifluoride β-diketonates and β-enaminoketonates,[13–19] discotic borolanes,[20] and boroxines.[21,22] Boron clusters containing carboranes, *closo*-boranes, and *closo*-carbaborates give rise to polar liquid crystals relevant for molecular electronic and nonlinear optical applications.[23–28] Boron clusters such as **1** and **2** have been utilized to probe the stabilization of thermotropic mesophases by Coulomb and dipolar interactions (Scheme 1).[23,26] For example, isosteric and isoelectronic replacement of the *apical* C–C bond in carbaborates **1a** by N-B (**1b**) not only increased the longitudinal dipole moment by an order of magnitude, but also stabilized the nematic (N) phase by 55 K.[23] However, reversal of the carbon position in the carbaborate cluster **2a** increased the dipole moment but led to a very high melting point and disappearance of the smectic A (SmA) phase.[26]

Another powerful tool in the design of liquid crystals is perfluoroalkyl chains, which show higher polarity and rigidity than alkyl chains favoring nanosegregation and formation of mesophases.[29] Terminal semifluorinated chains in combination with rod-like structures such as cyanobiphenyls,[30] alkoxybenzoates,[31] and Schiff's base systems[32] stabilize SmA and SmC phases and show high thermal

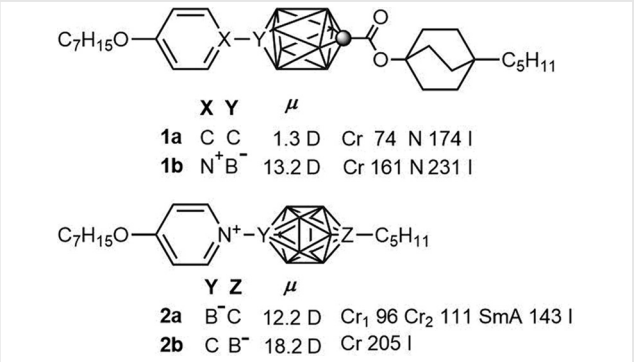

Scheme 1 Liquid crystalline boron clusters.[23,26]

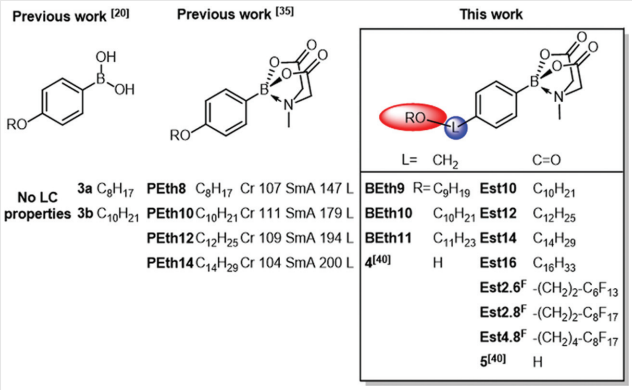

Figure 1 Boronic acid **3**,[20] liquid crystalline MIDA boronates **Peth**[35] and **Beth**; **Est** presented in this work.

stability. Furthermore, the successful application on bent-core structures such as naphthalene,[33] viologen, and oxadiazolyl bipyridine[34] was reported.

Previously, we disclosed that *p*-alkoxyphenyl boronates **PEth** carrying the *N*-methyliminodiacetic acid (MIDA) unit as a protecting group at boron displayed stable SmA mesophases in contrast to the corresponding boronic acids **3** with similar chain lengths (Figure 1).[35] Quantum-chemical calculations showed that the longitudinal dipole moment of the MIDA boronates **PEth** is three times larger than those of the boronic acids **3**. Furthermore, the computational study in combination with solid-state structures yielded dipole distributions and provided a model for the liquid crystalline self-assembly of these MIDA boronates **PEth**. In the previous work, mesophase induction was achieved by variation of the charge distribution in the "boron head group" and the phase type was governed mostly by the number of side chains,[35] i.e. exclusion of free volume.[36] We surmised that attaching a nonpolar (methylene) or polar (carboxylate) linker opposite to the MIDA unit at the aryl ring should affect both mesophase stability, i.e. clearing temperature, and temperature range of the mesophase. Furthermore, by utilizing the fluorophobic effect,[29] i.e. replacing flexible alkyl side chains by more rigid and more polar partially fluorinated side chains, the mesomorphic properties should be modified as well. In the current manuscript, we describe the dipole moment variation via linkers and side chains by synthesizing MIDA boronates **BEth** and **Est**.

Although protective group chemistry, subsequent functionalization and cross-coupling of MIDA boronates have been extensively studied,[37–39] and both precursors, 4-MIDA boronato benzylic alcohol **4** (L = CH_2) and 4-MIDA boronato benzoic acid **5** (L = C=O) respectively, are known compounds[40]; the corresponding ethers and esters are quite rare. Thus, we anticipated that the synthesis of compounds **BEth** and **Est** might not only lead to new insights from a materials perspective but also require new synthetic methods. Our results, which are reported below, show that this is indeed the case.

Results and Discussion

The synthesis of MIDA boronate benzyl ethers **BEth** is shown in Scheme 2. Commercially available 4-MIDA boronato benzylic alcohol **4** was treated with NaH and 1-bromodecane in DMF at room temperature following a method by Jin et al. (route A).[41]

However, after 16 h no trace of decylether **BEth10** could be detected. Thus, an alternative protocol was developed for the Williamson etherification (route B). 4-Bromobenzylbromide **6** was treated with NaH and the respective alcohol in DMF for 16 h at 0 °C and warmed to room temperature and the desired ethers **7a**,**b** were isolated in 73% and 69%, respectively. Subsequent reaction with *n*-BuLi and triisopropylborate in THF at –78 °C, followed by addition of MIDA in DMSO at 125 °C, yielded the MIDA boronates **Beth9** and **BEth11** in 65% and 63%, respectively, without any event.

Next, the synthesis of the esters **Est** was examined (Scheme 3). Jones oxidation of **4** provided the known MIDA boronate benzoic acid **5**.[40] Attempted esterification of **5** with 1-decanol under Steglich conditions with *N,N′*-dicyclohexylcarbodiimide (DCC) or 1-ethyl-3-(3-dimethylaminopropyl) carbodiimide (EDCI) and DMAP[42] did not meet with any success, even when different solvents were tested (for details, see Table S1, Supplementary Information). Also, the reaction of **5** with thionyl chloride followed by treatment with sodium decanolate did not give the desired product **Est10**. Next, Yamaguchi conditions were tested,[43] but no trace of the ester **Est10** could be detected. After these unsuccessful trials, we turned our attention to the Mitsunobu esterification (Scheme 3 and Table 1). Thus, acid **5** was treated with 1-decanol, triphenylphosphine, and diethyl azodicarboxylate (DEAD) in THF. Reaction monitoring by ^{1}H NMR revealed 20% conversion to the ester **Est10** after 14 h at room temperature (entry 1). Replacement of DEAD by diisopropyl azodicarboxylate (DIAD) and an increase of the temperature to 60 °C gave an increased yield of 40% of **Est10**, albeit with only 85% purity due to contamination with triphenylphosphine oxide, which could not be separated by column chromatography (entry 2). Despite variations of the workup procedure,[44] complete removal of triphenylphosphine oxide was not possible. Next, we tested a method by Boger[45] employing tri-*n*-butylphosphine, which gave 43% yield of the product **Est10** but still with low purity (80%; entry 3). In a final attempt, trimethylphosphine was employed together with DIAD in THF at room temperature. Luckily, this procedure provided the desired ester **Est 10** in 53% yield in the pure form (entry 4). In order to prevent oxidation of the trimethylphosphine, special

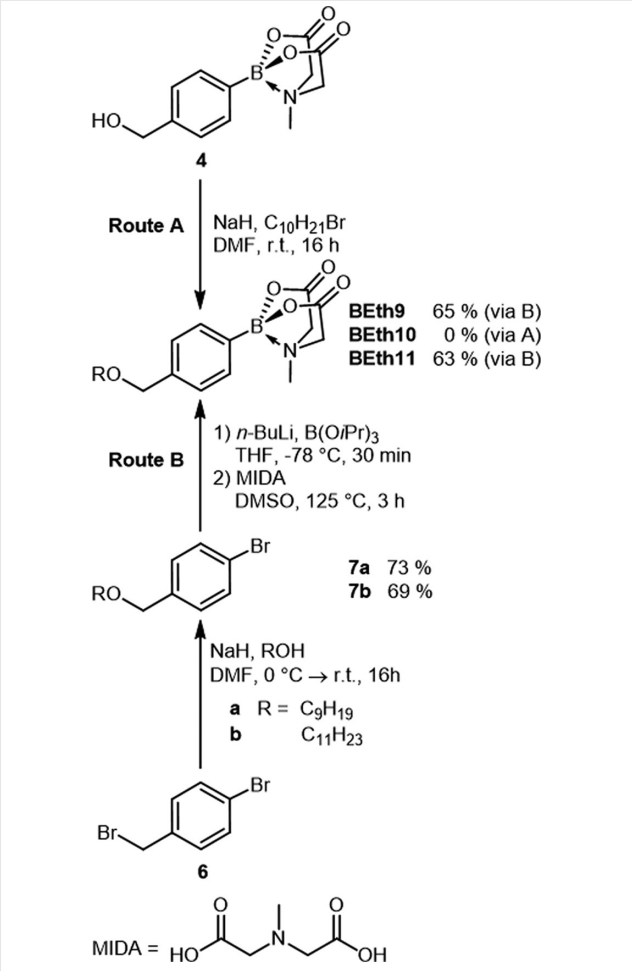

Scheme 2 Synthetic route of **BEth**.

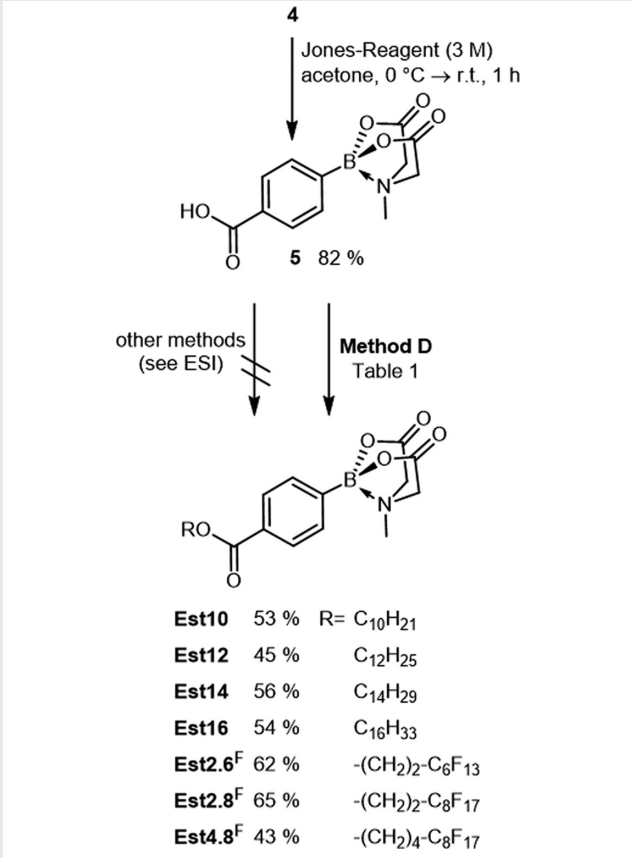

Scheme 3 Synthetic route of **Est**.

precautions, e.g. a rigorous Schlenk technique, must be taken to exclude oxygen. By using this optimized protocol, the homologous ester derivatives **Est12**, **Est14**, and **Est16** as well as the esters with fluorinated side chains **Est2.6^F**, **Est2.8^F**, and **Est4.8^F** could be obtained in 43–65% yield (Scheme 3).

Liquid crystalline properties of compounds **BEth** and **Est** were analyzed by differential scanning calorimetry (DSC), polarizing optical microscopy (POM), and X-ray diffraction [small-angle X-ray scattering (SAXS) and wide-angle X ray scattering (WAXS)]. The DSC results are summarized in Table 2. Benzylic ethers **BEth9** and **Beth11** showed enantiotropic mesomorphism in the DSC. Upon heating of benzylic ether **BEth9** with C_9H_{19} chains, an endothermal melting transition at 105 °C followed by isotropization at 147 °C were observed (Table 2).

Upon cooling, the mesophase reappeared at 146 °C and the glass transition at 102 °C was hardly visible. The derivative **BEth11** with $C_{11}H_{23}$ chains behaved similarly. In the series of esters **Est10**–**Est16**, the derivative **Est10** with $C_{10}H_{21}$ chains was nonmesomorphic and showed an isotropic melting transition at 131 °C (Table 2). In contrast, esters **Est12** and **Est14** displayed enantiotropic mesophases, e.g. for homologue **Est12** a crystallization at 74 °C, an endothermal melting transition at 134 °C, and an endothermal clearing transition at 152 °C were detected upon heating. In the cooling cycle, only isotropic to mesophase transitions at 152 °C and a glass transition at 62 °C were detected.

For all fluorinated derivatives **Est2.6^F**, **Est2.8^F**, and **Est4.8^F**, decomposition was observed during the first heating cycle. Melting transitions into the liquid crystalline phase were visible at 160 °C for the shortest chain-length **Est2.6^F**. The longer perfluoro derivative **Est2.8^F** melted at 176 °C, whereas **Est4.8^F** melted at 169 °C. Upon further heating, additional endothermal decomposition peaks were observed at 240 °C for **Est2.6^F**, 287 °C for **Est2.8^F**, and 268 °C for **Est4.8^F**. During subsequent heating and cooling cycles, no transitions were observed.

During our investigation using a polarizing optical microscope of benzyl ether **Beth9**, we observed uncharacteristic textures (Figure 2a); however, **Beth11** showed large

Table 1 Esterification of 5 under Mitsunobu reaction conditions[a] to decyl ester **Est10**

Entry	Reagents	Temp.	Method	Yield (purity[b])
1	DEAD, PPh_3	r.t.	A	20% (<85%)
2	DIAD, PPh_3	60 °C	B	40% (85%)
3	DIAD, PBu_3	r.t.	C	43% (80%)
4[c]	DIAD, PMe_3	r.t.	D	53% (>99%)

[a]1-Decanol, THF, 14 h.
[b]Determined by ^{1}H NMR.
[c]Schlenk conditions were applied.

Table 2 DSC results of different MIDA boronates: Phase transition temperatures *T* are given in °C and the transition enthalpies in kJ/mol[a]

Compound	Cycle	Cr1	*Tm*(Δ*H*)	Cr2	*T*(Δ*H*)	SmA	*Tc*(Δ*H*)	I
BEth9	2nd heat	•	105 (14.7)			•	147 (1.3)	•
	2nd cool	G	102 (–)			•	146 (–1.7)	•
BEth11	2nd heat	G	110 (–)			•	161 (1.4)	•
	2nd cool	G	108 (–)			•	158 (–1.7)	•
Est10	1st heat	•	131 (–)					•
Est12	2nd heat	G	74 (–32.2)	•	134 (46.8)	•	152 (3.7)	•
	2nd cool	G	62 (–)			•	152 (–3.1)	•
Est14	2nd heat	•	71 (6.3)	•	145 (12.4)	•	176 (1.0)	•
	2nd cool	•	63 (–5.1)	•	77 (–4.1)	•	176 (–1.0)	•
Est16	2nd heat	•	74 (12.4)	•	140 (11.6)	•	183 (0.9)	•
	2nd cool	•	64 (–14.5)			•	182 (–1.2)	•
Est2.6^F	1st heat	•	160 (24.9)			•	240 (6.7)	•[b]
Est2.8^F	1st heat	•	176 (27.1)			•	287(7.2)	•[b]
Est4.8^F	1st heat	•	169 (82.8)			•	268 (5.2)	•[b]

[a]Heating/cooling rate 10 K/min. Phase transitions were determined during 1st heating cycle for **Est10**, **Est2.6^F**, **Est2.8^F**, and **Est4.8^F**, and during 2nd heating/cooling for **BEth9**, **BEth11**, **Est12**, **Est14**, and **Est16**.
[b]Decomposition during 1st heating cycle.

areas of homeotropic alignment with small maltese cross-defects (Figure S6), despite the use of silylated slides. Furthermore, we observed a similar behaviour for MIDA boronates **Est12–16**, **Est2.6^F**, **Est2.8^F**, and **Est4.8^F**. While compounds **Est12** (Figure 2b) and perfluoro esters **Est2.6^F**, **Est2.8^F**, and **Est4.8^F** (Figure 2e, f) showed uncharacteristic textures, compounds **Est14** and **Est16** showed large areas of homeotropic alignment with small defects (Figure 2c).

A phenomenon we observed for all samples was the formation of filament-like textures after shearing of the cover glasses, indicating an SmA phase (Figure 2d). These observations are similar to the behavior of the previously published MIDA boronates.[35] With the observations under the polarizing microscope and the structural resemblance to our previously published boronates, we surmised a smectic mesophase. The findings of DSC experiments for perfluorinated derivatives **Est2.6^F**, **Est2.8^F**, and **Est4.8^F** are in accordance with observations under the polarizing microscope. We observed uncharacteristic textures for the perfluorinated derivatives **Est2.6^F**, **Est2.8^F**, and **Est4.8^F** upon heating and slow fading at higher temperatures. No textures were observed during later heating and cooling cycles. This was another indication for decomposition of the samples at high temperatures.

To obtain a deeper insight into the mesophase geometries, for one member of each series, SAXS and WAXS measurements were conducted (Table 3). The diffractogram of **BEth9** is shown in Figure 3a. In the small-angle area, the (001) reflection is displayed. Moreover, in the wide-angle area, a broad halo was visible. To clarify the phase geometries, temperature-dependent SAXS measurements were conducted. From the (001) X-ray diffractions for derivatives **BEth9** and **Est16**, the layer spacing *d* was calculated. The layer spacings with the corresponding temperatures are shown in Figure 3b.

During cooling, a gradual increase in the layer spacing was observed. This is a typical phenomenon observed for SmA phases, presumably due to decreasing interdigitation of side chains. During DSC measurements for perfluoro derivatives, we observed a decomposition of the compounds. Therefore, we were not able to gather sufficient data for evaluation from the SAXS measurement of **Est2.6^F**. Fortunately, it was possible to conduct temperature-dependent WAXS experiments before decomposition started. Similar to the above-discussed experiments, an increase of the layer spacing *d* during cooling was observed.

To compare the layer spacings among each series, we calculated the reduced layer spacing d_{red} from the layer spacing trend lines at the reduced clearing temperature ($0.95 \times T_c$). For comparison, the molecular lengths in the *all-trans*-configuration were estimated using the Avogadro program[46] (molecular mechanics, force field: MMFF94s). The molecular length of nonyl ether **BEth9** was determined between the outer most atoms to be 20.8 Å and the reduced layer spacing to be $d_{red} = 29.6$ Å. d_{red} is larger than the molecular length (*L*) but shorter than the twofold molecular length (2*L*), indicating an interdigitation of the side chains. However, the calculated layer spacing for full interdigitation is in good agreement with d_{red} ($d_{cal} = 31.5$ Å). For the alkoxy ester **Est16**, the reduced layer spacing d_{red} is 39.3 Å, which is in good agreement with the calculated value for fully interdigitated side chains ($d_{cal} = 38.1$ Å). Furthermore, the molecular length of perfluoro ester **Est2.6^F** was determined to be 21.1 Å and the reduced layer spacing d_{red} to be 36.9 Å.

To rationalize the large volume d_{red}, we propose that the fluorophobic effect as well as the steric demand of the fluorinated tails leads to nanosegregation and an unfavorable interdigitation of the chain as observed for derivatives with alkyl ethers (**BEth9**) and alkoxy esters (**Est16**), respectively (Figure 4a). Instead the core fragments are stacked as shown in Figure 4b.

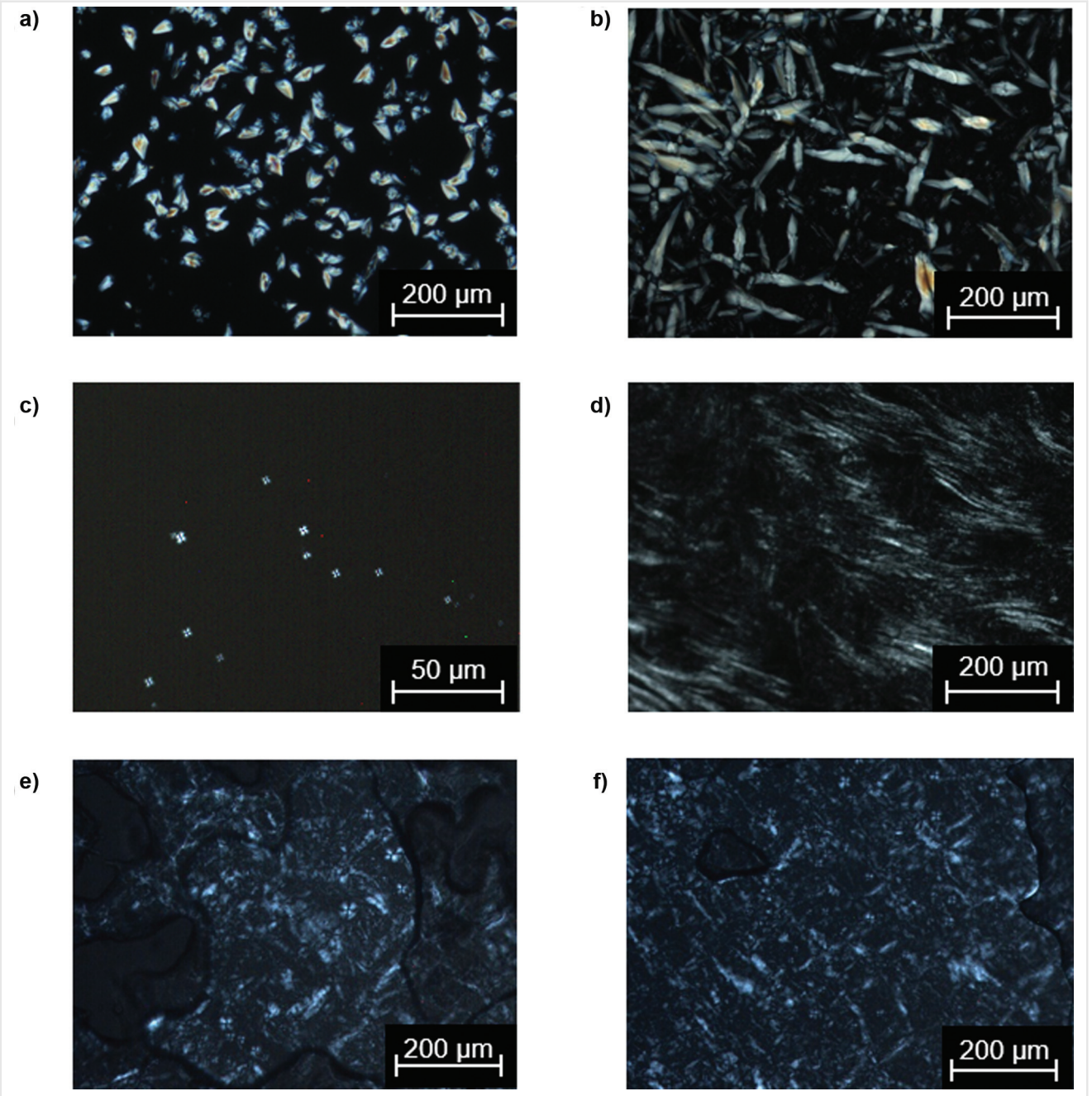

Figure 2 Observed POM textures of nonyl ether **BEth9** at 152 °C (**a**); dodecyl ester **Est12** at 150 °C (**b**); hexadecyl ester **Est16** at 165 °C (**c**); and after shearing (**d**); perfluorodecyl ester **Est2.8^F** at 230 °C (**e, f**) (200× magnification).

Upon comparison of MIDA boronate benzyl ethers **BEth9** and **BEth11** with the corresponding MIDA boronate aryl ethers **Peth**,[35] the additional methylene group did not affect the melting transition but decreased the clearing point considerably (compare, e.g., **PEth10** vs. **BEth9** and **PEth12** vs. **BEth11**) by 30 K.

In contrast, the additional "*anti-periplanar*" dipole introduced by the carboxylate moiety resulted in a slightly reduced longitudinal dipole moment. However, the slightly bent ester led to the appearance of a second crystalline phase (temperature range: 60–70 K) and an SmA phase (phase widths: 18–43 K) for **Est12**–**Est16**. However, the known tendency of

Table 3 XRD data of derivatives **BEth9**, **Est16**, and **Est2.6^F**

Compd.	Mesophase	*d* Values (Å), expt. (calcd.)	Miller indices
BEth9	SmA at 140 °C	30.2 (–)	(001)
		4.9	Halo
Est16	SmA at 150 °C	39.0 (–)	(001)
		4.40	Halo
Est2.6^F	SmA at 225 °C	38.6 (–)	(001)
		19.2 (19.3)	(002)
		12.8 (12.9)	(003)
		5.7	Halo

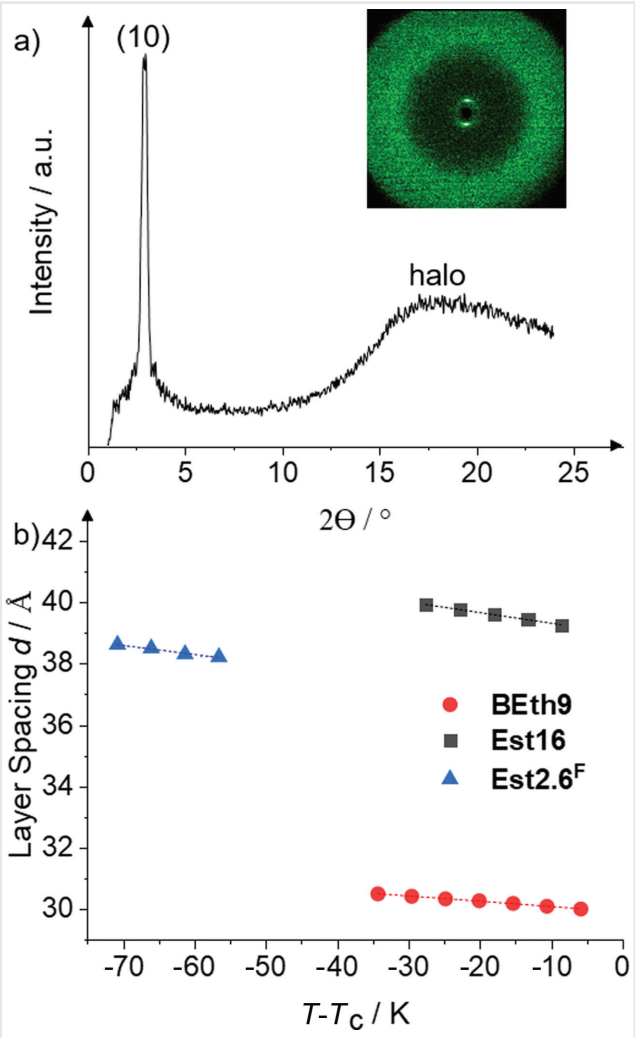

Figure 3 (a) WAXS diffractogram of **Beth9** at 140 °C and 2D X-ray pattern (inset). (b) Temperature-dependent layer spacing *d* of **Beth9**, **Est16**, and **Est2.6^F**.

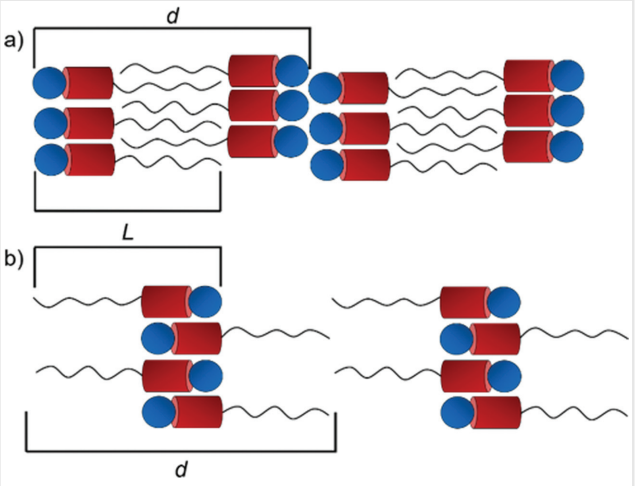

Figure 4 Packing model of MIDA boronates **BEth9**, **Est16** (a), and **Est2.6^F** (b).

fluorinated or partially fluorinated side chains to reduce the conformational mobility[29,47] significantly stabilized the SmA phase up to the thermal decomposition at 240–287 °C.

In addition, melting points also increased by 80–100 K and thus the overall mesophase widths increased up to 37 K as compared to the nonfluorinated analogues.

To obtain further insight into the packing model, we performed quantum-chemical calculations (for details, see the Experimental Section, quantum chemical calculations). In our previous studies, a negligible impact of chain length on the electronic core structure of MIDA boronates **PEth8**–**PEth14** was observed. This prompted us to use MIDA boronates with ethoxy side chains as model systems in the calculations. Here, we use the compound **BEth2** as a model for all compounds with a methylene linker and **Est2** as a model for all compounds with a carboxylate linker. One of the first findings of our computations was that the overall dipole moment of the two compounds was not strongly affected by the linker group. We calculated a value of 7.1 D for both **BEth2** and **Est2**, which is only slightly smaller than the dipole moment of alkoxy ether **PEth2** (7.6 D; Figure 5). More insight was provided by plotting the electrostatic potential of **BEth2**, **Est2**, and **PEth2** (Figure 6). The plot of **PEth2** (Figure 6c) indicates that there is no strong variation of the electrostatic potential in the vicinity of the phenyl oxygen, whereas **BEth2** and **Est2** (Figure 6a, b) show a strong contribution of the negatively charged oxygen atoms to the electrostatic potential. This will likely induce repulsive interactions between neighboring side chains and lead to decreased interdigitation of these.

Furthermore, ester **Est2** and ether **BEth2** exhibit a slightly bent structure of the side chain in comparison to nearly linear compound **PEth2**. This bending of **BEth2** and **Est2** leads to a larger occupied volume fraction and an unfavorable space filling in the liquid-crystalline phase, resulting in decreased clearing temperatures for benzyl

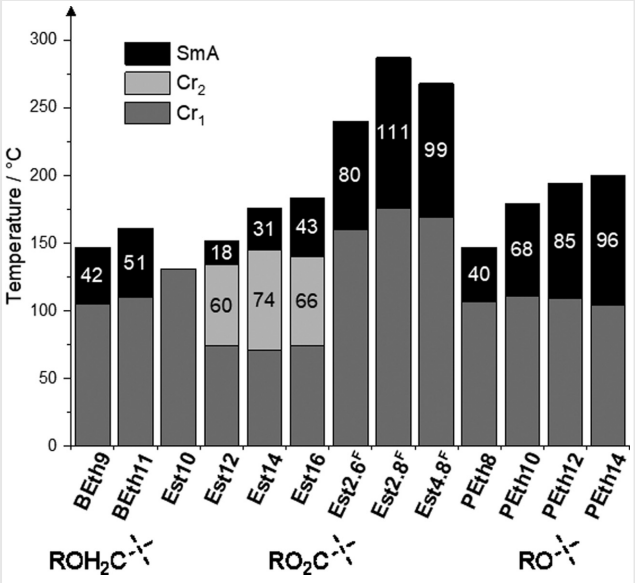

Figure 5 Phase transition diagram of MIDA boronates **Est10**–**Est16**, **Est2.6^F**, **Est2.8^F**, **Est4.8^F**, **BEth9**, **BEth11**, and **PEth8**–**PEth14**. Values for **PEth8**–**PEth14** were taken from Wöhrle et al.[35] for comparison.

ethers **BEth9** and **BEth11** and a second crystalline phase for alkyl esters **Est12**–**Est16**. The bending of MIDA boronate ester **Est2** formed in the calculations also explains why compounds **Est12**–**Est16** with alkyl side chains have lower melting and clearing points together with smaller phase widths as compared with the derivatives **Est2.6^F**, **Est2.8^F**, and **Est4.8^F** with partially fluorinated side chains. The fluorinated tails of **Est2.6^F**, **Est2.8^F**, and **Est4.8^F** are stiffer and more rigid than the alkyl chains of **Est2.6^F**, **Est2.8^F**, and **Est4.8^F**, and they tend to pack more tightly due to fluorine–fluorine interactions. Thus, even a short fluorinated tail and an overall shorter total chain length can outperform a much longer alkyl chain; see for example **Est16** vs. **Est2.6^F**.

Conclusions

In conclusion, a convenient synthetic access to both MIDA-boronate benzyl ethers **BEth9** and **BEth11** and MIDA boronate esters **Est10**–**Est16**, **Est2.6^F**, **Est2.8^F**, and **Est4.8^F**, respectively, has been developed. Key steps were Williamson etherification of 4-bromobenzyl bromide and late-stage borylation in the case of **BEth9** and **BEth11**, while MIDA boronate carboxylic acid **5** could be successfully esterified under Mitsunobu conditions to **Est10**–**Est16**, **Est2.6^F**, **Est2.8^F**, and **Est4.8^F**.

Except for compound **Est10**, all other MIDA boronates showed SmA phases, with particularly broad phases for MIDA boronate esters **Est2.6^F**, **Est2.8^F**, and **Est4.8^F** with partially fluorinated tails. Their packing mechanisms and different mesomorphic properties were compared with those of the known MIDA boronate alkoxy ethers **PEth8**–**PEth14** and rationalized by quantum-chemical calculations. Our results show that even unfavorable dipolar and electrostatic interactions as well as bending of a calamitic core can be overruled by attachment of fluorine tails resulting in the formation of broad mesophases. Thus the current work broadens the scope of MIDA boronates with respect to organic materials.

Experimental Section

NMR spectra were recorded on *Bruker Avance* 500 (^{1}H, 500 MHz; ^{13}C, 126 MHz), *Bruker Avance* 400 (^{1}H, 400 MHz; ^{13}C, 100 MHz), and *Bruker Avance* 300 (^{1}H, 300 MHz; ^{13}C, 75 MHz). All NMR spectra were recorded at room temperature and the calibration was done on the residual solvent peaks. For calibration of NMR spectra, the residual solvent peaks were used. FT-IR spectra were recorded on a *Bruker Vector* 22 FT-IR spectrometer with a MKII golden gate single reflection Diamond ATR system, at room temperature. POM was performed using an *Olympus BX50* polarizing microscope with a *Linkam TP93* central controller. DSC measurements were performed on a *Mettler Toledo DSC 822e* device in aluminum pans (40 µL) from *Mettler Toledo*. X-ray diffraction measurements (SAXS and WAXS) were conducted on a *Bruker Nanostar C* device with a HI-STAR detector using $Cu_{K\alpha}$ radiation (α = 1.5418 Å) calibrated to silver behenate. TLC was done on aluminum plates precoated with silica gel 60 F_{254} from Merck. Flash chromatography was conducted with silica gel from *Fluka* (grain size: 40–63 µm).

Materials

All commercial chemicals were used as received. Dry solvents were distilled under a nitrogen atmosphere using common drying agents prior to use. Moisture- and/or oxygen-sensitive reactions were conducted using common Schlenk techniques**.** The synthesis of MIDA,[48] 4-(6-methyl-4,8-dioxo-1,3,6,2-dioxazaborocan-2-yl) benzoic acid,[40] trimethylphosphine,[49,50] and ethyl 3-butenoate[51] were performed according to literature procedures.

Esterification: General Procedure

MIDA acid **5** (0.10 g, 0.36 mmol), DIAD (0.09 mL, 0.47 mmol), and the respective alcohol (0.47 mmol) were dissolved in dry THF (10 mL). Trimethylphosphine (0.05 mL, 0.47 mmol) was added and the reaction mixture was stirred overnight at room temperature. The solvent was removed under removed pressure. The crude product was purified by column chromatography (hexanes/ethyl acetate 1:3; R_f: 0.2) and Soxhlet extraction (hexane).

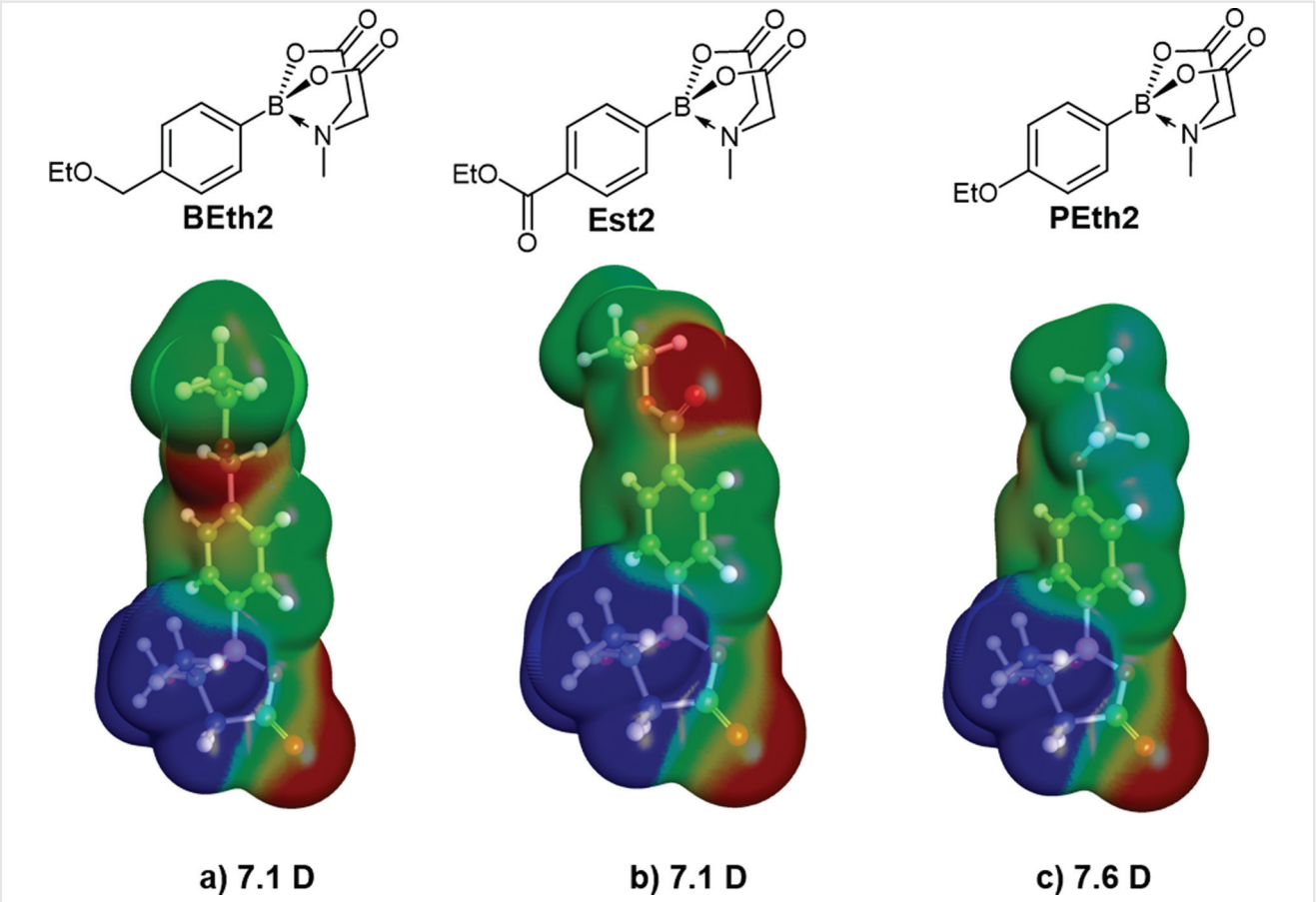

Figure 6 Visualization of the electrostatic potential of MIDA boronates **BEth2**, **Est2**, and **PEth2**. The electrostatic potential is color-coded (red = −1.9 eV to blue 1.9 eV) on an isosurface of the electron density (0.0067 $Å^{-3}$).

Decyl-4-(6-methyl-4,8-dioxo-1,3,6,2-dioxazaborocan-2-yl)benzoate (Est10)

The general esterification procedure was followed with **5** and 1-decanol to give **Est10** as a white solid (80 mg, 53%).

^{1}H NMR (400 MHz, $CDCl_3$): δ = 8.05 (d, J = 8.2 Hz, 2H, 3-H), 7.61 (d, J = 8.2 Hz, 2H, 2-H), 4.32 (t, J = 6.7 Hz, 2H, OCH_2), 3.95 (d, J = 16.4 Hz, 2H, 1′-H), 3.78 (d, J = 16.4 Hz, 2H, 1′-H), 2.55 (s, 3H, NCH_3), 1.71–1.82 (m, 2H), 1.20–1.49 (m, 14H, CH_2), 0.84–0.93 (m, 3H, CH_3), ppm. ^{13}C NMR (101 MHz, $CDCl_3$): δ = 166.7 (C=O), 166.52 (C-5), 132.25 (C-2), 132.04 (C-4), 129.29 (C-3), 65.32 (OCH_2), 61.90 (C-1′), 47.45 (NCH_3), 31.89, 29.53, 29.30, 28.72, 26.03, 22.67 (CH_2), 14.10 (CH_3) ppm. FT-IR (ATR): 2956 (w), 2924 (s), 2854 (w), 2178 (w), 2039 (w), 1761 (s), 1718 (s), 1562 (w), 1507 (w), 1458 (w), 1430 (w), 1396 (w), 1337 (w), 1272 (vs), 1221 (s), 1186 (w), 1112 (s), 1039 (vs), 997 (s), 890 (w), 843 (s), 803 (w), 767 (s), 711 (w), 648 (w), 594 (w), 547 (w), 513 (w), 482 (w) cm^{-1}. MS (ESI): m/z = 440 $[M + Na]^+$. HRMS (ESI) (m/z): $[M + Na]^+$ calcd. for $C_{22}H_{32}BNO_6Na$: 440.2219, found: 440.2210. CHN analysis calcd. (%) for $C_{22}H_{32}BNO_6$ (417.31): C 63.32 H 7.73, N 3.36; found: C 62.34, H 7.47 N 2.83.

Dodecyl-4-(6-methyl-4,8-dioxo-1,3,6,2-dioxazaborocan-2-yl) benzoate (Est12)

The general esterification procedure was followed with **5** and 1-dodecanol to give **Est12** as a white solid (73 mg, 45%).

^{1}H NMR (500 MHz, $CDCl_3$): δ = 8.05 (d, J = 8.2 Hz, 2H, 3-H), 7.61 (d, J = 8.2 Hz, 2H, 2-H), 4.31 (t, J = 6.7 Hz, 2H, $-OCH_2$), 4.02 (d, J = 16.4 Hz, 2H, 1′-H), 3.80 (d, J = 16.4 Hz, 2H, 1′-H), 2.55 (s, 3H, NCH_3), 1.72–1.80 (m, 2H, OCH_2), 1.20–1.38 (m, 16H, CH_2), 1.39–1.47 (m, 2H, OCH_2CH_2), 0.87 (t, J = 6.9 Hz, 3H, CH_3) ppm. ^{13}C NMR (126 MHz, $CDCl_3$): δ = 167.4 (C=O), 166.8 (C-5), 132.5 (C-2), 132.2 (C-4), 129.5 (C-3), 65.6 (OCH_2), 62.1 (C-1′), 47.8 (NCH_3), 32.1, 29.89, 29.87, 29.83, 29.79, 29.59, 29.54, 28.94, 26.2, 22.8 (CH_2), 14.38 (CH_3) ppm. FT-IR (ATR): 2955 (w), 2923 (s), 2854 (s), 1763 (s), 1719 (vs), 1562 (s), 1508 (w), 1459 (w), 1396 (w), 1396 (w), 1337 (w),

1274 (vs), 1222 (s), 1186 (w), 1113 (w), 1041 (s), 996 (s), 890 (w), 843 (w), 767 (w), 711 (w), 650 (w), 594 (w) cm^{-1}. MS (ESI): $m/z = 468$ $[M + Na]^+$. HRMS (ESI) (m/z): $[M + Na]^+$ calcd. for $C_{24}H_{36}BNO_6Na$: 468.2532, found: 468.2530. CHN analysis calcd. (%) for $C_{24}H_{326}BNO_6$ (445.36): C 64.73 H 8.15, N 3.15; found: C 64.73, H 8.22 N 3.23.

Tetradecyl-4-(6-methyl-4,8-dioxo-1,3,6,2-dioxazaborocan-2-yl) benzoate (Est14)

The general esterification procedure was followed with **5** and 1-tetradecanol to give **Est14** as a white solid (96 mg, 56%).

^{1}H NMR (700 MHz, $CDCl_3$): $\delta = 8.06$ (d, $J = 7.7$ Hz, 2H, 3-H), 7.61 (d, $J = 7.7$ Hz, 2H, 2-H), 4.32 (t, $J = 6.7$ Hz, 2H, –OCH_2), 3.95 (d, $J = 16.3$ Hz, 2H, 1′-H), 3.79 (d, $J = 16.3$ Hz, 2H, 1′-H), 2.56 (s, 3H, –NCH_3), 1.74–1.80 (m, 2H, –OCH_2CH_2), 1.40–1.46 (m, 2H, –$OCH_2CH_2CH_2$), 1.21–1.38 (m, 20H, CH_2), 0.88 (t, $J = 7.1$ Hz, 3H, CH_3) ppm. ^{13}C NMR (176 MHz, $CDCl_3$) $\delta = 166.8$ (C=O) 166.5 (C-5), 132.3 (C-2), 132.0 (C-4), 129.3 (C-3), 65.3 (OCH_2), 61.9 (C-1′), 47.5 (NCH_3), 31.92, 29.70, 29.68, 29.66, 29.60, 29.55, 29.36, 29.30, 28.72, 26.04, 22.70 (CH_2), 14.13 (CH_3) ppm. FT-IR (ATR): 2922 (vs), 2853 (w), 1762 (s), 1719 (s), 1562 (w), 1459 (w), 1396 (w), 1337 (w), 1275 (s), 1221 (w), 1186 (w), 1114 (w), 1040 (s), 996 (w), 890 (w), 843 (w), 767 (w), 711 (w), 595 (w) cm^{-1}. MS (ESI): $m/z = 496$ $[M + Na]^+$. HRMS (ESI) (m/z): $[M + Na]^+$ calcd. for $C_{26}H_{40}BNO_6Na$ 496.2846, found: 497.2877. CHN analysis calcd. (%) for $C_{26}H_{40}BNO_6$ (473,42): C 65.96, H 8.52, N 2.96; found: C 65.88, H 8.68 N 2.99.

Hexadecyl 4-(6-methyl-4,8-dioxo-1,3,6,2-dioxazaborocan-2-yl) benzoate (Est16)

The general esterification procedure was followed with **5** and 1-hexadecanol to give **Est16** as a white solid (98 mg, 54%).

^{1}H NMR (700 MHz, $CDCl_3$): $\delta = 8.05$ (d, $J = 8.0$ Hz, 2H, 3-H), 7.61 (d, $J = 8.0$ Hz, 2H, 2-H), 4.32 (t, $J = 6.7$ Hz, 2H, –OCH_2), 4.01 (d, $J = 16.3$ Hz, 2H, 1′-H), 3.80 (d, $J = 16.4$ Hz, 2H, 1′-H), 2.56 (s, 3H, NCH_3), 1.73–1.80 (m, 2H, OCH_2), 1.39–1.47 (m, 2H, OCH_2CH_2), 1.21–1.38 (m, 24H, CH_2), 0.87 (t, $J = 7.0$ Hz, 3H, CH_3) ppm. ^{13}C NMR (176 MHz, $CDCl_3$) $\delta = 167.1$ (C=O), 166.5 (C-5), 132.3 (C-2), 132.0 (C-4), 129.3 (C-3), 65.3 (OCH_2), 61.9 (C-1′), 47.6 (NCH_3), 29.31, 31.93, 29.70, 29.69, 29.66, 29.62, 29.56, 29.37, 28.72, 26.04, 22.70, (CH_2), 14.14 (CH_3) ppm. FT-IR (ATR): 2917 (vs), 2850 (s), 2165 (w), 1762 (s), 1719 (w), 1467 (w), 1277 (w), 1114 (w), 1041 (w), 995 (w), 842 (w), 767 (w), 711 (w) cm^{-1}. MS (ESI): $m/z = 501$ $[M]^+$. HRMS (ESI) (m/z): $[M + Na]^+$ calcd. for $C_{28}H_{44}BNO_6Na$ 524.3159, found: 524.3165. CHN analysis calcd. (%) for $C_{28}H_{44}BNO_6$ (501.47): C 67.06, H 8.84, N 2.79; found: C 66.81, H 8.70 N 2.70.

3,3,4,4,5,5,6,6,7,7,8,8,8-Tridecafluorooctyl 4-(6-methyl-4,8-dioxo-1,3,6,2-dioxazaborocan-2-yl) benzoate (Est2.6^F)

The general esterification procedure was followed with **5** and 1,1,2,2-*H*-perfluorooctanol to give **Est2.6^F** as a white solid (139 mg, 62%).

^{1}H NMR (500 MHz, $CDCl_3$): $\delta = 8.08$ (d, $J = 7.9$ Hz, 2H, 2-H), 7.66 (d, $J = 7.9$ Hz, 2H, 3-H), 4.68 (t, $J = 6.4$ Hz, 2H, OCH_2), 3.99 (d, $J = 16.4$ Hz, 2H, 1′-H), 3.83 (d, $J = 16.4$ Hz, 2H, 1′-H), 2.54–2.73 (m, 2H, OCH_2CH_2), 2.60 (s, 3H, NCH_3) ppm. ^{13}C NMR (101 MHz, $(CD_3)_2CO$): $\delta = 169.1$ (C=O), 166.6 (C-5), 133.7 (C-2), 131.2 (C-4), 129.5 (C-3), 63.0 (C-1′), 57.6 (OCH_2), 48.4 (NCH_3), 30.1 (p, $J = 39.0$ Hz, OCH_2CH_2) ppm. ^{19}F NMR (376 MHz, $CDCl_3$): $\delta = -125.90$ to -126.19 (m), -123.33 to -123.63 (m), -122.61 to -122.98 (m), -121.64 to -121.93 (m), -113.29 to -113.57 (m), -80.76 (tt, $J = 9.9$ Hz, 2.6 Hz) ppm. FT-IR (ATR): 1770 (s), 1730 (s), 1455 (w), 1397 (w), 1337 (w), 1275 (s), 1232 (s), 1187 (vs), 1143 (s), 1121 (s), 1036 (s), 999 (s), 964 (w), 889 (w), 841 (s), 810 (w), 782 (w), 765 (s), 733 (w), 708 (s), 651 (w), 598 (w), 567 (w), 531 (w), 501 (w), 454 (w), 440 (w) cm^{-1}. MS (ESI): $m/z = 622$ $[M - H^+]^-$. HRMS (ESI) (m/z): $[M - H^+]^-$ calcd. for $C_{20}H_{14}BF_{13}NO_6$ 622.0705, found: 622.0697. CHN analysis calcd. (%) for $C_{20}H_{15}BF_{13}NO_6$ (623.13): C 38.55, H 2.43, N 2.25; found: C 38.51, H 2.63 N 2.13.

3,3,4,4,5,5,6,6,7,7,8,8,9,9,10,10,10-Heptadecafluorooctyl 4-(6-methyl-4,8-dioxo-1,3,6,2-dioxazaborocan-2-yl)benzoate (Est2.8^F)

The general esterification procedure was followed with **5** and 1,1,2,2-*H*-perfluorodecanol to give **Est2.8^F** as a white solid (169 mg, 65%).

^{1}H NMR (500 MHz, $(CD_3)_2CO$): $\delta = 8.02$ (d, $J = 8.1$ Hz, 2H, 2-H), 7.70 (d, $J = 8.1$ Hz, 2H 3-H), 4.69 (t, $J = 6.1$ Hz, 2H, OCH_2), 4.40 (d, $J = 17.0$ Hz, 2H, 1′-H), 4.20 (d, $J = 17.0$ Hz, 2H, 1′-H), 2.82 (s, 3H, NCH_3), 2.75–2.94 (m, 2H, OCH_2CH_2) ppm. ^{13}C NMR (126 MHz, $(CD_3)_2CO$): $\delta = 169.2$ (C=O), 166.6 (C-5), 133.7 (C-2), 131.2 (C-4), 129.5 (C-3), 62.9 (C-1′), 57.6 (OCH_2), 48.4 (NCH_3), 30.1 (p, $J = 38.7$ Hz, OCH_2CH_2) ppm. ^{19}F NMR (376 MHz, $(CD_3)_2CO$): $\delta = -126.54$ to -126.81 (m), -123.83 to -124.16 (m), -123.01 to -123.36 (m), -121.94 to -122.55 (m), -113.63 to -113.99 (m), -81.64 (t, $J = 10.1$ Hz) ppm. FT-IR (ATR): 1766 (s), 1731 (s), 1455 (w), 1397 (w), 1372 (w), 1334 (w), 1274 (s), 1201 (vs), 1146 (s), 1115 (s), 1071 (w), 1036 (s), 1003 (s), 961 (w), 878 (w), 860 (w), 842 (w), 766 (w), 738 (w), 710 (w), 654 (w), 621 (w), 595 (w), 559 (w), 530 (w), 499 (w), 441 (w), 419 (w) cm^{-1}. MS (ESI): $m/z = 746$ $[M + Na]^+$. HRMS (ESI) (m/z): $[M + Na]^+$ calcd. for $C_{22}H_{15}BF_{17}NO_6Na$ 746.0617, found: 746.0614. CHN analysis calcd. (%) for $C_{22}H_{15}BF_{17}NO_6$ (723.15): C 36.54, H 2.09, N 1.94; found: C 36.56, H 2.03 N 1.80.

5,5,6,6,7,7,8,8,9,9,10,10,11,11,12,12,12-Heptadecafluorododecyl 4-(6-methyl-4,8-dioxo-1,3,6,2-dioxazaborocan-2-yl)benzoate (Est4.8^F)

The general esterification procedure was followed with **5** and **10** to give **Est4.8^F** as a white solid (116 mg, 43%).

^{1}H NMR (500 MHz, $(CD_3)_2CO$): δ = 8.01 (d, J = 8.3 Hz, 2H, 2-H), 7.69 (d, J = 8.3 Hz, 2H), 4.37–4.43 (m, 4H, 1′-H, OCH_2), 4.19 (d, J = 17.1 Hz, 2H, 1′-H), 2.77 (s, 3H, NCH_3), 2.37 (tt, J = 19.6 Hz, 8.0 Hz, 2H, 4″-H), 1.92–2.00 (m, 2H, 2″-H), 1.79–1.89 (m, 2H, 3″-H) ppm. ^{13}C NMR (126 MHz, $(CD_3)_2CO$): δ = 17.9 (C-3″), 28.8 (C-2″), 30.1 (p, J = 39.0 Hz, C-4″) 48.4 (NCH_3), 62.9 (C-1′), 64.9 (OCH_2), 129.4 (C-3), 131.8 (C-4), 133.7 (C-2), 166.9 (C-5), 169.2 (C=O) ppm. ^{19}F NMR (376 MHz, $CDCl_3$): δ = −125.95 to −126.13 (m), −123.30 to −123.53 (m), −122.51 to −122.77 (m), −121.50 to −122.00 (m), −114.25 to −114.49 (m), −80.72 (t, J = 9.5 Hz), ppm. FT-IR (ATR): 1765 (s), 1719 (s), 1463 (w), 1396 (w), 1370 (w), 1333 (w), 1273 (s), 1199 (vs), 1146 (vs), 1114 (s), 1035 (s), 1002 (s), 961 (s), 928 (w), 888 (w), 842 (w), 807 (w), 792 (w), 767 (s), 736 (w), 705 (s), 654 (s), 621 (w), 595 (w), 559 (w), 529 (w), 460 (w) cm^{-1}. MS (ESI): m/z = 774 $[M + Na]^+$. HRMS (ESI) (m/z): $[M + Na]^+$ calcd. for $C_{24}H_{19}BF_{17}NO_6Na$ 774.0930, found: 774.0914. CHN analysis calcd. (%) for $C_{24}H_{19}BF_{17}NO_6$ (751.20): C 38.37, H 2.55, N 1.86; found: C 38.45, H 2.64 N 1.75.

Etherification: General Procedure

Sodium hydride (0.50 g, 12.5 mmol) was placed in the reaction flask and washed with pentane (3 × 5 mL). DMF (20 mL) was added and the suspension was cooled to 0 °C. The respective alcohol (11.0 mmol) was added dropwise and the reaction mixture was stirred for 30 min at 0 °C. 4-Bromobenzylbromide **9** (2.50 g, 10.0 mmol) was added in portions and the mixture was stirred at room temperature for 16 h. The solvent was evaporated, water (50 mL) was added, and the product was extracted with CH_2Cl_2 (3 × 50 mL). The combined organic layers were dried over $MgSO_4$. Evaporation of the solvent gave the title compound which was used without further purification.

1-Bromo-4-((nonyloxy)methyl)benzene (7a)

The general etherification procedure was followed with **6** and 1-nonanol to give **7a** as a white solid (2.29 g, 73%).

^{1}H NMR (400 MHz, $CDCl_3$): δ = 7.42–7.50 (m, 2H, 2-H), 7.17–7.25 (m, 2H, 3-H), 4.44 (s, 2H, 5-H), 3.45 (t, J = 6.6 Hz, 2H, –OCH_2), 1.53–1.67 (m, 2H, –OCH_2CH_2), 1.18–1.42 (m, 12H, CH_2), 0.80–0.94 (m, 3H, CH_3) ppm. ^{13}C NMR (101 MHz, $CDCl_3$): δ = 137.8 (C-4), 131.4 (C-2), 129.2 (C-3), 121.3 (C-1), 72.1 (C-5), 70.7 (–OCH_2), 31.89, 29.75, 29.56, 29.48, 29.28, 26.19, 22.68, (CH_2), 14.11 (CH_3), ppm. MS (EI): m/z = 312 $[M]^+$. HRMS (ESI) (m/z): $[M + Na]^+$ calcd. for $C_{16}H_{25}BrONa$: 335.0981, found: 335.0974.

1-Bromo-4-((undecyloxy)methyl)benzene (7b)

The general etherification procedure was followed with **6** and 1-undecanol to give **7b** as a white solid (2.49 g, 65%).

^{1}H NMR (400 MHz, $CDCl_3$): δ = 7.43–7.49 (m, 2H, 2-H), 7.17–7.25 (m, 2H, 3-H), 4.44 (s, 2H, 5-H), 3.45 (t, J = 6.6 Hz, 2H, –OCH_2), 1.51–1.66 (m, 2H, –OCH_2CH_2), 1.19–1.41 (m, 16H, CH_2), 0.83–0.92 (m, 3H, CH_3), ppm. ^{13}C NMR (101 MHz, $CDCl_3$): δ = 137.8 (C-4), 131.4 (C-2), 129.2 (C-3), 121.3 (C-1), 72.1 (C-5), 70.7 (–OCH_2), 31.92, 29.75, 29.62, 29.60, 29.48, 29.35, 26.19, 22.70 (CH_2), 14.12 (CH_3), ppm. MS (EI): m/z = 340 $[M]^+$. HRMS (ESI) (m/z): $[M + Na]^+$ calcd. for $C_{18}H_{29}BrONa$: 363.1294, found: 363.1290.

Benzyl Ether Boronate Preparation: General Procedure

The respective alkoxy-bromo-benzene **6** (2.93 mmol) was dissolved in dry THF (20 mL) and cooled to −78 °C. n-BuLi (1.9 mL, 4.69 mmol, 2.5 M) was added and the mixture was stirred for 30 min. Triisopropyl borate (1.1 mL, 4.69 mmol) was added and the reaction was allowed to warm up to room temperature over 2 h. A solution of MIDA (1.3 g, 8.79 mmol) in abs. DMSO (18 mL, 0.5 M) was added and the mixture was refluxed for 2 h. The reaction mixture was poured into water and extracted with CH_2Cl_2 (3 × 50 mL). Combined organic layers were washed with brine (50 mL), dried with $MgSO_4$, and the solvent was evaporated. The crude product was purified by flash chromatography (hexanes/ethyl acetate 1:1; R_f: 0.3).

6-Methyl-2-{4-[(nonyloxy)methyl]phenyl}-1,3,6,2-dioxazaborocane-4,8-dione (BEth9)

The general etherification procedure was followed for benzyl ether boronate preparation with **7a** to give **BEth9** as a white solid (741 mg, 65%).

^{1}H NMR (400 MHz, $CDCl_3$): δ = 7.47 (d, J = 7.7 Hz, 2H, 2-H) 7.34 (d, J = 7.7 Hz, 2H, 3-H), 4.48 (s, 2H, 5-H), 4.11 (d, J = 16.8 Hz, 2H, 1′-H), 3.78 (d, J = 16.7 Hz, 2H, 1′-H), 3.48 (t, J = 6.7 Hz, 2H, CH_2O), 2.51 (s, 3H, NCH_3), 1.57–1.67 (m, 2H, CH_2CH_2O), 1.21–1.40 (m, 12H, CH_2), 0.83–0.92 (m, 3H, CH_3), ppm. ^{13}C NMR (101 MHz, $CDCl_3$): δ = 167.4 (C=O), 140.7 (C-4), 132.3 (C-2), 127.5 (C-3), 72.7 (C-5), 70.9 (-OCH_2), 61.8 (C-1′), 47.49 (NCH_3), 29.77, 29.57, 29.52, 29.28, 26.20, 22.67 (CH_2), 14.11 (CH_3) ppm. FT-IR (ATR): 2924 (w), 2853 (w), 1746 (vs), 1613 (w), 1457 (w), 1697 (w), 1338 (w), 1292 (s), 1229 (s), 1115 (w), 1099 (w), 1037 (s),

990.92 (s), 890 (w), 865 (w), 807 (w), 710 (w), 653 (w), 593 (w), 548 (w), 491 (w), 458 (w) cm^{-1}. MS (ESI): $m/z = 412$ $[M + Na]^+$. HRMS (ESI) (m/z): $[M + Na]^+$ calcd. for $C_{21}H_{32}BNO_5Na$: 412.2269, found: 412.2290. CHN analysis calcd. (%) for $C_{21}H_{32}BNO_5$ (389.30): C 64.79 H 8.29, N 3.60; found: C 64.66, H 7.99 N 3.49.

6-Methyl-2-{4-[(undecyloxy)methyl]phenyl}-1,3,6,2-dioxazaborocane-4,8-dione (BEth11)

The general etherification procedure was followed for benzyl ether boronate preparation with **7b** to give **BEth11** as a white solid (770 mg, 63%).

^{1}H NMR (400 MHz, $CDCl_3$): $\delta = 7.48$ (d, $J = 7.7$ Hz, 2H, 2-H), 7.36 (d, $J = 7.7$ Hz, 2H, 3-H), 4.49 (s, 2H, 5-H), 3.94–4.10 (m, 2H, 1′-H), 3.77 (d, $J = 16.1$ Hz, 2H, 1′-H), 3.48 (t, $J = 6.7$ Hz, 2H, $-OCH_2$), 2.53 (s, 3H, $-NCH_3$), 1.54–1.67 (m, 2H, $-OCH_2CH_2$), 1.19–1.42 (m, 16H, CH_2), 0.84–0.91 (m, 3H, CH_3), ppm. ^{13}C NMR (101 MHz, $CDCl_3$): $\delta = 167.2$ (C=O), 140.7 (C-4), 132.3 (C-2), 127.5 (C-3), 72.7 (C-5), 70.9 ($-OCH_2$), 61.8 (C-1′), 47.4 (NCH_3), 31.92, 29.77, 29.63, 29.52, 29.34, 26.21, 22.69, (CH_2), 14.12 (CH_3) ppm. FT-IR (ATR): 2922 (s), 2853 (w), 1761 (vs), 1612 (w), 1457 (w), 1397 (w), 1338 (w), 1293 (s), 1230 (s), 1115 (w), 1100 (w), 1038 (s), 991 (w), 890 (w), 865 (w), 807 (w), 710 (w), 653 (w), 593 (w), 548 (w), 491 (w), 458 (w) cm^{-1}. MS (ESI): $m/z = 440$ $[M + Na]^+$. HRMS (ESI) (m/z): $[M + Na]^+$ calcd. for $C_{23}H_{36}BNO_5Na$: 440.2579, found: 440.2596. CHN analysis calcd. (%) for $C_{23}H_{36}BNO_5$ (417.35): C 66.19 H 8.69, N 3.36; found: C 65.94, H 8.55 N 3.27.

Quantum Chemical Calculations

We employed Møller–Plesset second-order perturbation theory (MP2) and a def2-TZVPP basis set and appropriate auxiliary basis sets for efficient two-electron integral evaluation.[52–54] Full-structure optimizations were carried out at this level of theory and dipole moments and electrostatic potentials were evaluated from the relaxed one-electron density. The TURBOMOLE program package[55,56] was used throughout; graphical representations were generated by the TmoleX program (Version 4.5.2).[57]

Funding Information

Generous financial support by the Ministerium für Wissenschaft, Forschung und Kunst des Landes Baden-Württemberg, the Fonds der Chemischen Industrie, the Deutsche Forschungsgemeinschaft, and the Carl-Schneider-Stiftung Aalen (shared instrumentation grant) is gratefully acknowledged.

Supporting Information

Supporting information for this article is available online at http://doi.org/10.1055/s-0040-1715900.

References

(1) Mula, S.; Frein, S.; Russo, V.; Ulrich, G.; Ziessel, R.; Barberá, J.; Deschenaux, R. *Chem. Mater.* **2015**, *27*, 2332.
(2) Florian, A.; Mayoral, M. J.; Stepanenko, V.; Fernández, G. *Chemistry* **2012**, *18*, 14957.
(3) Olivier, J.-H.; Barberá, J.; Bahaidarah, E.; Harriman, A.; Ziessel, R. *J. Am. Chem. Soc.* **2012**, *134*, 6100.
(4) Benstead, M.; Rosser, G. A.; Beeby, A.; Mehl, G. H.; Boyle, R. W. *New J. Chem.* **2011**, *35*, 1410.
(5) Benstead, M.; Rosser, G. A.; Beeby, A.; Mehl, G. H.; Boyle, R. W. *Photochem. Photobiol. Sci.* **2011**, *10*, 992.
(6) Olivier, J.-H.; Camerel, F.; Ulrich, G.; Barberá, J.; Ziessel, R. *Chemistry* **2010**, *16*, 7134.
(7) Frein, S.; Camerel, F.; Ziessel, R.; Barberá, J.; Deschenaux, R. *Chem. Mater.* **2009**, *21*, 3950.
(8) Camerel, F.; Ulrich, G.; Barberá, J.; Ziessel, R. *Chemistry* **2007**, *13*, 2189.
(9) Cavero, E.; Lydon, D. P.; Uriel, S.; de la Fuente, M. R.; Serrano, J. L.; Giménez, R. *Angew. Chem. Int. Ed.* **2007**, *46*, 5175.
(10) Cavero, E.; de la Fuente, M. R.; Beltrán, E.; Romero, P.; Serrano, J. L.; Giménez, R. *Chem. Mater.* **2007**, *19*, 6230.
(11) Camerel, F.; Bonardi, L.; Schmutz, M.; Ziessel, R. *J. Am. Chem. Soc.* **2006**, *128*, 4548.
(12) Camerel, F.; Bonardi, L.; Ulrich, G.; Charbonnière, L.; Donnio, B.; Bourgogne, C.; Guillon, D.; Retailleau, P.; Ziessel, R. *Chem. Mater.* **2006**, *18*, 5009.
(13) Bando, Y.; Sakurai, T.; Seki, S.; Maeda, H. *Chem. Asian J.* **2013**, *8*, 2088.
(14) Terashima, Y.; Takayama, M.; Isozaki, K.; Maeda, H. *Chem. Commun.* **2013**, *49*, 2506.
(15) Mayoral, M. J.; Ovejero, P.; Campo, J. A.; Heras, J. V.; Oliveira, E.; Pedras, B.; Lodeiro, C.; Cano, M. *J. Mater. Chem.* **2011**, *21*, 1255.
(16) Turanova, O. A.; Turanov, A. N.; Lapaev, D. V.; Gnezdilov, O. I.; Lobkov, S. V.; Galyametdinov, Y. G. *Russ. J. Gen. Chem.* **2006**, *76*, 730.
(17) Turanova, O. A.; Kal'dyaeva, E. V.; Gnezdilov, O. I.; Nikitin, S. I.; Turanov, A. N. *Russ. J. Gen. Chem.* **2010**, *80*, 258.
(18) Sánchez, I.; Mayoral, M. J.; Ovejero, P.; Campo, J. A.; Heras, J. V.; Cano, M.; Lodeiro, C. *New J. Chem.* **2010**, *34*, 2937.
(19) Sánchez, I.; Núñez, C.; Campo, J. A.; Torres, M. R.; Cano, M.; Lodeiro, C. *J. Mater. Chem. C* **2014**, *2*, 9653.
(20) Tatum, L. A.; Johnson, C. J.; Fernando, A. A. P.; Ruch, B. C.; Barakoti, K. K.; Alpuche-Aviles, M. A.; King, B. T. *Chem. Sci.* **2012**, *3*, 3261.
(21) Wöhrle, T.; Baro, A.; Laschat, S. *Materials* **2014**, *7*, 4045.
(22) Belloni, M.; Manickam, M.; Wang, Z.-H.; Preece, J. A. *Mol. Cryst. Liq. Cryst.* **2003**, *399*, 93.
(23) Ringstrand, B.; Kaszynski, P. *J. Mater. Chem.* **2010**, *20*, 9613.
(24) Ringstrand, B.; Kaszynski, P. *J. Mater. Chem.* **2011**, *21*, 90.
(25) Pecyna, J.; Kaszyński, P.; Ringstrand, B.; Bremer, M. *J. Mater. Chem. C* **2014**, *2*, 2956.
(26) Pecyna, J.; Ringstrand, B.; Domagała, S.; Kaszyński, P.; Woźniak, K. *Inorg. Chem.* **2014**, *53*, 12617.
(27) Ringstrand, B.; Monobe, H.; Kaszynski, P. *J. Mater. Chem.* **2009**, *19*, 4805.
(28) Jankowiak, A.; Sivaramamoorthy, A.; Pociecha, D.; Kaszyński, P. *RSC Adv.* **2014**, *4*, 53907.

(29) Tschierske, C. *Top. Curr. Chem.* **2012**, *318*, 1.
(30) Jang, J. Y.; Park, Y. W. *Liq. Cryst.* **2013**, *40*, 511.
(31) Ciastek, S.; Szymańska, K.; Kaszyński, P.; Jasiński, M.; Pociecha, D. *Liq. Cryst.* **2018**, *45*, 11.
(32) Liu, Z.; Zhang, J.; Li, T.; Yu, Z.; Zhang, S. *J. Fluorine Chem.* **2013**, *147*, 36.
(33) Kovářová, A.; Kozmík, V.; Svoboda, J.; Novotná, V.; Glogarová, M.; Pociecha, D. *Liq. Cryst.* **2012**, *39*, 755.
(34) Pibiri, I.; Beneduci, A.; Carraro, M.; Causin, V.; Casella, G.; Corrente, G. A.; Chidichimo, G.; Pace, A.; Riccobono, A.; Saielli, G. *J. Mater. Chem. C* **2019**, *7*, 7974.
(35) Wöhrle, T.; Gündemir, R.; Frey, W.; Knecht, F.; Köhn, A.; Laschat, S. *Chemistry* **2017**, *23*, 4149.
(36) Goodby, J. W.; Davis, E. J.; Mandle, R. J.; Cowling, S. J. Handbook of Liquid Crystals, Vol. 1, 2nd ed. Wiley-VCH: Weinheim; **2014**, 231–260.
(37) Uno, B. E.; Gillis, E. P.; Burke, M. D. *Tetrahedron* **2009**, *65*, 3130.
(38) Gillis, E. P.; Burke, M. D. *J. Am. Chem. Soc.* **2007**, *129*, 6716.
(39) Fujii, S.; Chang, S. Y.; Burke, M. D. *Angew. Chem. Int. Ed.* **2011**, *50*, 7862.
(40) Gillis, E. P.; Burke, M. D. *J. Am. Chem. Soc.* **2008**, *130*, 14084.
(41) Jin, C.; Lee, H.; Lee, S.; Kim, I.; Jung, Y. *Synlett* **2007**, *2007*, 2695.
(42) Butschies, M.; Haenle, J. C.; Tussetschläger, S.; Laschat, S. *Liq. Cryst.* **2013**, *40*, 52.
(43) Inanaga, J.; Hirata, K.; Saeki, H.; Katsuki, T.; Yamaguchi, M. *Bull. Chem. Soc. Jpn.* **1979**, *52*, 1989.
(44) Lukin, K.; Kishore, V.; Gordon, T. *Org. Process Res. Dev.* **2013**, *17*, 666.
(45) Boger, D. L.; Johnson, D. S.; Yun, W. *J. Am. Chem. Soc.* **1994**, *116*, 1635.
(46) Hanwell, M. D.; Curtis, D. E.; Lonie, D. C.; Vandermeersch, T.; Zurek, E.; Hutchison, G. R. *J. Cheminf.* **2012**, *4*, 17.
(47) Haenle, J. C.; Stöckl, Y.; Forschner, R.; Haenle, E.; Laschat, S. *ChemPhysChem* **2018**, *19*, 2758.
(48) Ballmer, S. G.; Gillis, E. P.; Burke, M. D. *Org. Synth.* **2009**, *86*, 344.
(49) Wolfsberger, W.; Schmidbaur, H. *Synth. React. Inorg. Met.-Org. Chem.* **1974**, *4*, 149.
(50) Kornath, A.; Neumann, F.; Oberhammer, H. *Inorg. Chem.* **2003**, *42*, 2894.
(51) Ramachandran, P. V.; Nicponski, D.; Kim, B. *Org. Lett.* **2013**, *15*, 1398.
(52) Weigend, F.; Häser, M. *Theor. Chem. Acc.* **1997**, *97*, 331.
(53) Weigend, F.; Ahlrichs, R. *Phys. Chem. Chem. Phys.* **2005**, *7*, 3297.
(54) Weigend, F.; Häser, M.; Patzelt, H.; Ahlrichs, R. *Chem. Phys. Lett.* **1998**, *294*, 143.
(55) TURBOMOLE V7 1 2016, a development of University of Karlsruhe and Forschungszentrum Karlsruhe GmbH, 1989–2007, TURBOMOLE GmbH, since 2007; http://www.turbomole.com (accessed Aug 6, 2020).
(56) Furche, F.; Ahlrichs, R.; Hättig, C.; Klopper, W.; Sierka, M.; Weigend, F. *WIREs Comput. Mol. Sci.* **2014**, *4*, 91.
(57) Steffen, C.; Thomas, K.; Huniar, U.; Hellweg, A.; Rubner, O.; Schroer, A. *J. Comput. Chem.* **2010**, *31*, 2967.